Tracking Solutions for Mobile Robots: Evaluating Positional Tracking using Dual-axis Rotating Laser Sweeps

Sebastian P. Kleinschmidt, Christian S. Wieghardt and Bernardo Wagner

Real Time Systems Group, Institute of Systems Engineering, Leibniz Universität Hannover,
Appelstraße 9A, 30167 Hannover, Germany

Keywords: Tracking Technologies, Marker Tracking, Dual-axis Rotating Laser Sweeps.

Abstract: This paper provides a comprehensive introduction into state of the art marker-based tracking methods. There-fore, optical, magnetic, acoustic and inertial tracking are described and evaluated. All presented approaches are compared regarding accuracy, resolution, tracking volume, measurement rate and outdoor and indoor suit-ability. Additionally, typical technical limitations are mentioned for each system according to their functional principle.

As a technology with increasing potential for mobile robotics, we evaluate the achievable accuracy for pose tracking using dual-axis rotating laser sweeps as used in modern tracking systems for virtual reality applica-tions.

1 INTRODUCTION

In many applications, the pose of an object, a robot or an instrument needs to be determined as accurate as possible. Examples of such applications are medical engineering, augmented reality and mobile robotics. A detailed overview of tracking systems in medical applications is presented in (Birkfellner et al., 2008). In general, there are two basic solutions for determin-ing and tracking the pose of an object: Marker- and non marker-based systems. Due to higher accuracy, marker-based tracking systems have been established as the standard solution for pose measurements which can be used as ground truth for many research areas to evaluate the performance of developed algorithms. This paper gives a general overview of tracking sys-tems, which can be used in robotic applications.

This paper is organized as follows: The first sec-tion introduces evaluation criteria which can be used to compare state of the art marker-based tracking sys-tems. Then, the functional principles of different sys-tems as optical, magnetic, acoustic and inertial sys-tems are described. Subsequently, a comparison of the approaches is presented. The results are given in a comprehensive table. The paper ends with an eval-uation of a tracking system based on dual-axis rotat-ing laser sweeps. Experiments are performed using a trackable handheld device as well as a Pioneer 2 robot.

2 EVALUATION CRITERIA

All tracking systems considered in this paper will be evaluated based on the criteria presented in this sec-tion. If possible, we will quantify the results by speci-fications of commercial tracking systems or scientific publications.

Accuracy: According to ISO 5725, accuracy consists of *trueness* and *precision*. *Trueness* describes how close the mean of a set of measurements results to the *true value*, whereas *precision* describes the degree of scattering of the set of measurements. In tracking applications, *trueness* and *precision* may vary if the observed object is static or moving. Based on this fact, to evaluate tracking systems, it is necessary to differentiate between *static accuracy* and *dynamic ac-curacy*:

Static Accuracy: Static accuracy describes the accu-racy which can be achieved for a non-moving object.
Dynamic Accuracy: Analogue to the static accuracy, the dynamic accuracy is used for moving objects.

Resolution: The resolution of a tracking system is the smallest yet to distinguish difference in position and orientation which can be measured by the system.

Tracking Volume: The space in which a tracking system tracks objects, is called tracking volume. This tracking volume is described by geometric primitives, for which tracking is provided within defined accu-racy boundaries. The achievable accuracy may vary within this volume.

Measurement Rate: The measurement rate defines how many pose updates can be generated in a defined time period.

Indoor and Outdoor Suitability: Based on the function principle of the used tracking system, the system can be affected by external factors such as direct sunlight. Therefore, not all systems are equally suited for outdoor applications and need a controlled environment.

3 OPTICAL SYSTEMS

Traditional optical tracking systems consist of one or more cameras which are placed rigidly in the environment. The tracking volume is defined by the resulting overlapping field of view (fov) of the cameras. To track the position of a marker, the marker has to be visible in at least two cameras with a direct line-of-sight. Except are tracking approaches using predefined pattern such as fiducial marker which can be tracked by a single camera (see Section 3.1).

The accuracy of an optical system is mainly determined by the resolution of the used cameras, the fov given by the used lenses, the distance to the measured markers and the distance between the cameras in case of using multiple cameras.

The measurement rate is limited by the framerate of the cameras and can be further limited by the processing time which is needed to identify the maker or pattern structure. In case of using multiple cameras, the cameras need to be time synchronized. To simplify the identification of the marker position in the camera images, typical markers are coated with a reflective material which is illuminated by light sources arranged around the camera lenses (LEDs in most applications). To further facilitate the marker identification and prevent the influence of ambient light, the light sources often emit light in the infrared spectrum (e.g. 850 nm) which is filtered by an optical band-pass filter in front of the camera lenses.

Besides passive concepts, there are also active markers which are mostly battery powered and equipped with a light source (e.g. LEDs) inside the marker enclosure. There are also optical tracking systems which work without cameras such as laser tracking systems. In this kind of systems, the cameras are replaced by rotating planes of coherent lasers light which are detected using an array of photosensors. Laser based systems are described at the end of this section.
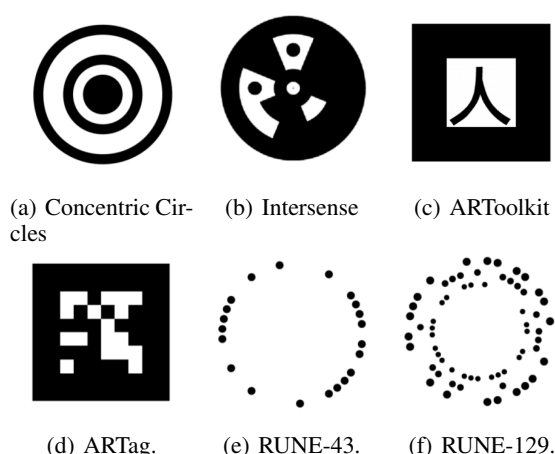

(a) Concentric Circles   (b) Intersense   (c) ARToolkit

(d) ARTag.   (e) RUNE-43.   (f) RUNE-129.

Figure 1: Examples of common fiducial markers (Bergamasco et al., 2011).

3.1 Single View Systems

The most basic setup for an optical tracking system is a single camera setup. Because tracking is not possible using triangulation with a spherical marker being visible in only one camera, it is necessary to use marker with predefined pattern as fiducial marker.

Besides typical spherical markers, it is common for simple applications to use fiducial markers as augmented reality tags or other predefined patterns. These markers are placed in the camera's fov as a point of reference. The resulting transformation between the pose of the marker and the camera can then be computed using conventional algorithms that solve the perspective-n-point problem. Typical applications for the usage of fiducial marker are augmented reality applications in mobile applications where virtual models are rendered into the camera image based on the computed transformation between the camera and the AR-Tag. Examples of fiducial markers are shown in Figure 1.

The accuracy of tracking a *Metaio* marker using a single camera has been evaluated in (Pentenrieder et al., 2006) using a simulated ground truth. The accuracy of Metaio marker detected by a simulated 640×480 (15 fps) camera has been evaluated from different distances and from different rotation angles.

The accuracy of optical tracking with an AR-ToolKit fiducial marker has been evaluated in (Abawi et al., 2004) using a camera with a resolution of 640×480 (15 fps). The systematic error was given by 2 cm in a distance of 20 cm and increases at higher distances.

The tracking volume for fiducial maker tracking is limited by the fov and the resolution of the used camera. The setup for a single camera tracking is sim-
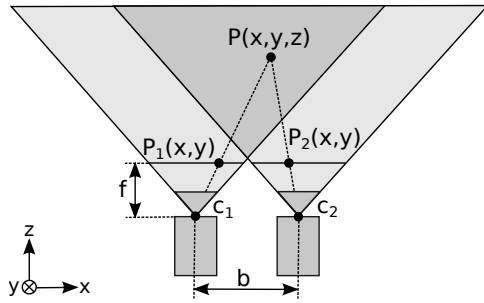
Figure 2: The basic setup of a stereo tracking system. The resulting tracking volume is marked dark gray.

ple because no time synchronization between different cameras needs to be performed and there is only an intrinsic calibration of one camera necessary. It is possible to determine the 6-dof transformation of a marker inside the camera's fov.

3.2 Stereo View Systems

Stereo-based tracking systems consist of two cameras which are placed in a rigid geometric relation to each other, and therefore have to be extrinsically and intrinsically calibrated. Figure 2 shows the basic setup of a stereo tracking system.

To triangulate the distance of a marker, both cameras need to be time synchronized. The depth of a marker Z given its disparity d can then be computed as follows (Szeliski, 2010):

$$Z = f\frac{b}{d}. \tag{1}$$

The theoretical depth resolution of a stereo camera system has been evaluated in (Mikko Kyt, 2011) and can be computed for the overlapping fov of both cameras:

$$dZ = \frac{Z^2}{fb}dp_x. \tag{2}$$

The theoretical depth resolution of a stereo system dZ depends on the focal length f, the baseline between both cameras b and the disparity accuracy dp_x. For a constant image resolution, dp_x increases with a growing fov wherefore the depth resolution impair.

While a small baseline b minimizes the regions of the image, where partial occlusions can occur, the depth uncertainty grows, because of a small triangulation angle. In contrast, a large baseline b increases the chance of an object only to be visible in one image but also increases the depth accuracy. Commercial stereo systems reach an accuracy of about 0.35 mm in a tracking volume up to approx. 1.6 m^3 (Andrew D. Wiles and Frantz, 2004).

Because the tracking volume is limited to the overlapping area of both cameras, the resulting tracking volume is smaller than the tracking volume which could be achieved with a single view system.

3.3 Multi-view Systems

In multi-view systems (*also known as multi-view stereo*), the marker must be visible in at least two cameras at the same time to perform triangulation. While depth estimation is already possible with two cameras, matching more images can be used to increase the tracking volume and make the system more robust against occlusions. One major factor for gaining high accuracy is to track objects with two cameras at perpendicular line of sights and small distances to the objects. Therefore, stereo view systems have a limited tracking volume with high accuracy. Whereas multi-view systems can easily deploy additional cameras in the tracking volume to increase such conditions, not for a significant higher accuracy, but for a larger high accurate tracking volume.

3.4 Laser Systems

Laser tracking systems are optical systems which work without the usage of cameras (in contrast to the optical approaches presented before). Instead of using passive or active markers which are detected in a camera image, the markers are replaced with an array of photosensors in a known geometric arrangement which are illuminated by two or more rotating planes of coherent lasers light. Therefore, the concept is also named dual-axis rotating laser sweeps, because every emitter is rotating two different laser planes. The position of the sensor array relative to the emitter is computed by sampling the position of the laser plane and the signal from the photosensors (Birkfellner et al., 2008).

While the outdoor suitability of laser-based tracking systems is determined by the wavelength and the power of the emitting light source, the possible tracking volume is mainly determined by the emitting angles of the laser planes which are rotated. Besides, the maximal distance between tracked device and the emitting base station is limited by the power of the emitting light source. The static resolution, which is achieved by a commercial laser tracking system, is given with 0.1 *mm* at a distance of 1 *m* (*laserBird 2 by Ascension Technology Corporation* working at a measurement rate of 250 *Hz* (Ascension Technology Corporation, 2000).

While laser tracking systems are not often used in medical applications (Birkfellner et al., 2008), they are interesting for head tracking in virtual reality applications based on the possible high frame rate and
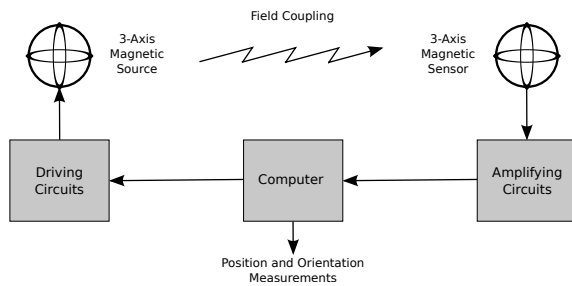
Figure 3: Magnetic coupling (based on figure presented in (Raab et al., 1979)).

low latency (which is necessary to avoid simulator sickness). Laser-based systems have become a highly available consumer product due to the usage in the HTC Vive virtual reality headset. Whereas the HTC Vive includes two controllers in addition to the headset, the system can be extended by stand alone trackable devices called HTC Trackers, which provide 6-dof tracking information. When this paper was written, the HTC Tracker were not yet available for purchase.

4 MAGNETIC SYSTEMS

Magnetic tracking systems consist of multiple magnetic emitters and one or more sensors whose position and orientation are tracked. In most systems, the source has three orthogonal coils which generate individual perpendicular magnetic fields and induce currents in the three orthogonal coils of the sensor (Raab et al., 1979). The amplitudes of the nine measured currents result in the position of the sensor, a comparison delivers the orientation. Small changes of the source position and orientation are determined and the previous measurements are updated. There are also alternative methods that use just two coils (Paperno et al., 2001) or a magnet (Hu et al., 2007) as a source. The basic structure of a magnetic tracking system is presented in Figure 3.

There are altering current (AC) and direct current (DC) based magnetic tracking systems. In AC systems, a signal sequence on a high carrier frequency wave is transmitted. The signal induces eddy currents in conductive materials nearby and therefore also small local electromagnetic fields which interfere with the measurements. DC-based magnetic systems generate pulsed constant magnetic fields. That prevents disturbances by conductive materials since eddy currents vanish fast enough. Whereas, constant magnetic fields such as the Earth's fields or caused by ferromagnetic materials can vary the measurements.

Hence, the trueness of the magnetic tracking strongly depends on its environment.

Since the induced field penetrates all sorts of materials, the tracking does not depend on a direct line-of-sight and are therefore not affected by occlusions. The method is also independent of lightning condition, thus is not restricted to indoor utilization.

Commercial magnetic tracking systems achieve a static precision of 0.76 *mm* RMS and 0.15° resp. RMS at a distance of 762 *mm* (*FASTRACK by Polhemus Inc.* (Polhemus, 2017a)). The system has a measurement rate of 120 *Hz* and a latency of 4 *ms*. The resolution is given by 0.0058 *mm* and 0.0026° at a distance of 304.8 *mm* and rapidly decreases with the displacement between source and sensor. At a distance of 3048 *mm* only a resolution of 40.64 *mm* and 2.96° resp. can be achieved. The range is limited to 10 feet but can be extended to 30 feet. There are also wireless magnetic tracking systems available e.g. (*PATRIOT WIRELESS by Polhemus Inc.* (Polhemus, 2017b)). They support a higher range, but suffer a loss in accuracy.

5 ACOUSTIC SYSTEMS

Acoustic tracking systems use the duration of ultrasonic waves to determine the position of the marker. For this purpose, the object is equipped with an ultrasonic transmitter as a marker while receivers are placed statically on defined locations in the environment. The position of a transmitter can then be determined by triangulating the time of flight of the ultrasonic waves.

Based on the limited propagation speed of ultrasonic waves in air (c≈ $343\frac{m}{s}$ at 20°C) the maximal update rate f is limited according to Equation 3. Because the propagation speed depends on the environmental conditions like temperature and pressure, the measurement of the time of flight needs to be fused with other sensors measuring these influencing factors to determine the correct distance. Furthermore, the time of flight can be affected by obstacles between the transmitter and the receiver.

$$f = \frac{c}{d} \quad (3)$$

The propagation speed c for different gases can be computed according to Equation 4.

$$c = \sqrt{\frac{\kappa \cdot p}{\rho}} = \sqrt{\kappa \cdot R \cdot T}, \quad (4)$$

with the adiabatic exponent κ, the pressure of the gas p, and the density of the gas ρ and R being the general gas constant.

The work presented in (Priyantha et al., 2000) describes a system called *Cricked* whose setup is inverse to the description above: The emitter are placed static in an indoor environment and the receivers are kept mobile on a robot for position tracking. The system achieves a location granularity of 4x4 square feet (Priyantha et al., 2000).

(Ward et al., 1997) presents a system called *Active Bats* which operates in a volume of $1100\ m^3$ using 256 ultrasonic receivers. The trueness of *Active Bats* is given with 9 *cm* for 95 % of the measurements with an update rate of 25 *Hz* (Hightower and Borriello, 2001) (Ward et al., 1997).

Compared to other tracking solutions, the price of an ultrasonic based tracking system is low (the price of each device used for the *Cricked* system costs less than 10 USD (Priyantha et al., 2000)). The propagation speed limits the update rate of systems based on ultrasonic time of flight measurements. Ultrasonic based systems are inaccurate compared to other tracking systems, can be disturbed by reflecting ultrasonic signals and are therefore not often used in state of the art applications.

6 INERTIAL SYSTEMS

Inertial navigation systems (INSs) use inertial measurement units (IMUs) as markers with no external tracking system to track the position of an object starting from a known initial position and orientation with a known initial velocity. These initial information are then combined with the output of the IMU to compute the position, velocity and attitude of the object (NovAtel, 2014). An IMU typically consists of a three-axis gyroscope and a three-axis accelerometer. Furthermore, there are also hybrid IMUs (magnetic, angular rate and gravity - MARG) available which include an additional three-axis magnetometer. INSs are divided into two different categories (Noriega-Manez, 2007) (Woodman, 2007):

- Stable Platform Systems *(also known as Gimbal-Mounted or Mechanized Systems)*

- Strap-Down Systems

Stable Platform Systems are mounted on a platform using gimbals to isolate the IMU from any external rotational motion (Woodman, 2007). The gyroscopes of the IMU are then used to measure occurring rotations to keep the platform's rotation static regarding a global frame of reference using servo motors. The orientation of the system can then be determined by reading the servo encoders. The position of the system is computed by double integrating the
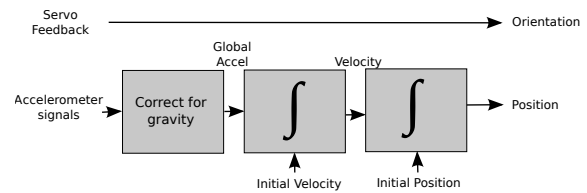

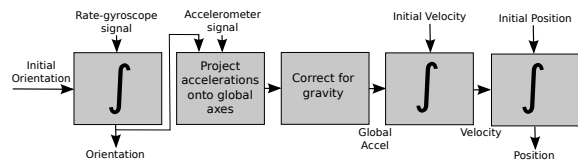Figure 4: Stable platform inertial navigation algorithm (based on figure presented in (Woodman, 2007)).

Figure 5: Strapdown inertial navigation algorithm (based on figure presented in (Woodman, 2007)).

acceleration which has to be corrected regarding gravity before integration. The basic structure of a stable platform inertial navigation algorithm is shown in Figure 4.

Strap-Down Systems are mounted directly onto the object with no additional mechanic structures and are therefore smaller than stable platform systems. In contrast to stable platform systems, strap-down systems can be rotated regarding the global frame and the accelerometer needs to be transformed into the global frame to correct the gravity. The position of the system can then be computed by double integrating the accelerometer signal (see Figure 5).

Signals from an IMU can typically be processed at a high measurement rate (e.g. 200 *Hz*) (NovAtel, 2014). Because the signals are measured directly at the object, there is no line-of-sight between the marker and an external device necessary.

If the bias error of the accelerometer is not removed, the error will be integrated twice as part of the mechanization process which will lead to a quadratic error in position computation (NovAtel, 2014). The same applies for the double integration of measurement noise and an error-prone compensation of gravity. Because the integration of the accelerometer signals is error-prone, the resulting position is strongly affected by drift. The average error in position for a *Xsens Mtx IMU* was given with 150 *m* after 60 *s* of operation (Woodman, 2007). For drift reduction, the IMU signal often gets merged with additional sensor signals as an absolute positioning system (e.g. GPS for outdoor applications or optical systems for indoor applications, see Section 3). A full introduction to inertial navigation systems (INSs) with a trial on error sources can be found in (Woodman, 2007) (NovAtel, 2014).

7 EVALUATION

Because a comprehensive evaluation of all presented tracking systems would exceed the scope of this paper, this section will focus on laser-based tracking as presented in Section 3.4. More precisely, positional tracking using dual-axis rotating laser sweeps will be evaluated, which recently gains importance for the robotic community due to virtual reality end consumer products such as the HTC Lighthouse tracking system, which drastically reduces the necessary investment costs. As a result, laser based systems become a widely available alternative to expensive multi-view camera systems. Consequently, the applicability of tracking robots using an HTC Lighthouse tracking system will be evaluated. The mathematical foundation of tracking using dual-axis rotating laser sweeps is presented in detail in (Islam et al., 2016). An outline of the underlying mathematics will be presented in the following section.

7.1 Architecture

Each vertical and horizontal swipe ends with an individual synchronization pulse indicating the starting position of the specific laser plane. The time between the individual synchronization pulse and the moment when the light hits a photodiode is measured and can be used to determine the horizontal and vertical angles φ_n and θ_n of the n-th photodiode according to Equation 5 and 6:

$$\varphi_n = \frac{t_{h,sync} - t_{h,n}}{t_{total}} \cdot 2\pi \tag{5}$$

$$\theta_n = \frac{t_{v,sync} - t_{v,n}}{t_{total}} \cdot 2\pi, \tag{6}$$

with $t_{h,n}$ and $t_{v,n}$, the points in time when the associated laser plane passes the photodiode, $t_{h,sync}$ and $t_{v,sync}$ when the corresponding synchronization signals trigger and t_{total}, the total time one laser plane takes for a complete revolution.

The pose of a rigid body with three rigid points at defined relative angles and distances as shown in Figure 6 can be computed as follows: The points A, B and C can be described in spherical coordinates by the following vectors $\mathbf{x}_A$, $\mathbf{x}_B$ and $\mathbf{x}_C$:

$$\mathbf{x}_A = \begin{pmatrix} r_A, & \varphi_A, & \theta_A \end{pmatrix}^T \tag{7}$$

$$\mathbf{x}_B = \begin{pmatrix} r_B, & \varphi_B, & \theta_B \end{pmatrix}^T \tag{8}$$

$$\mathbf{x}_C = \begin{pmatrix} r_C, & \varphi_C, & \theta_C \end{pmatrix}^T. \tag{9}$$

Whereas φ_n and θ_n of every point can be computed according to Equation 5, the distances r_n needs to be computed by solving a system of non-linear equations
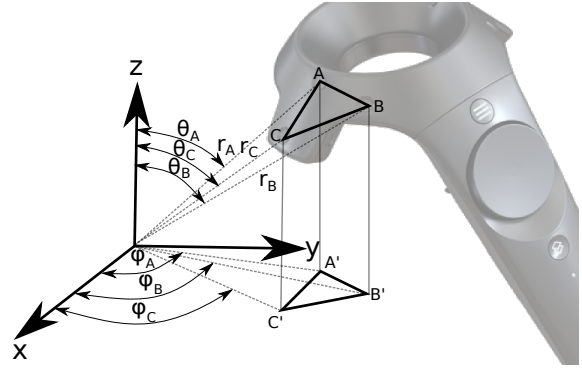

Figure 6: Illustration of the sensor triangle (cf. (Islam et al., 2016)).

which can be set by applying the law of cosines triangle:

$$r_A^2 + r_B^2 - 2 \cdot r_A \cdot r_B \cdot cos(\alpha_{AB}) - \overline{AB}^2 = 0 \tag{10}$$

$$r_B^2 + r_C^2 - 2 \cdot r_B \cdot r_C \cdot cos(\alpha_{BC}) - \overline{BC}^2 = 0 \tag{11}$$

$$r_A^2 + r_C^2 - 2 \cdot r_A \cdot r_C \cdot cos(\alpha_{AC}) - \overline{AC}^2 = 0. \tag{12}$$

The distances $\overline{AB}$, $\overline{BC}$ and $\overline{AC}$ of the rigid body are constant and are assumed to be known. To complete the set of Equations, $cos(\alpha_{AB})$, $cos(\alpha_{BC})$ and $cos(\alpha_{BC})$ need to be computed using the dot product according to Equation 13:

$$r_A \cdot r_B \cdot cos(\alpha_{AB}) = x_A x_B + y_A y_B + z_A z_B. \tag{13}$$

With respect to the vectors given in Equation 7, the cartesian coordinates can be computed using the spherical vectors as follows:

$$x_n = r_n \cdot sin(\theta_n) \cdot cos(\varphi_n) \tag{14}$$

$$y_n = r_n \cdot sin(\theta_n) \cdot sin(\varphi_n) \tag{15}$$

$$z_n = r_n \cdot cos(\theta_n). \tag{16}$$

After inserting Equation 14 to 16 in Equation 13, $cos(\alpha_{AB})$, $cos(\alpha_{BC})$ and $cos(\alpha_{BC})$ can be computed according to:

$$\begin{aligned} cos(\alpha_{AB}) = {} & sin(\theta_1) \cdot cos(\varphi_1) \cdot sin(\theta_2) \cdot cos(\varphi_2) \\ & + sin(\theta_1) \cdot sin(\varphi_1) \cdot sin(\theta_2) \cdot sin(\varphi_2) \\ & + cos(\theta_1) \cdot cos(\theta_2) \end{aligned} \tag{17}$$
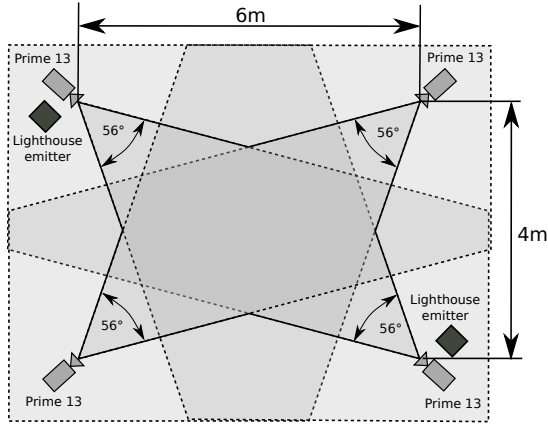
$$\begin{aligned} cos(\alpha_{BC}) = {} & sin(\theta_2) \cdot cos(\varphi_2) \cdot sin(\theta_3) \cdot cos(\varphi_3) \\ & + sin(\theta_2) \cdot sin(\varphi_2) \cdot sin(\theta_3) \cdot sin(\varphi_3) \\ & + cos(\theta_2) \cdot cos(\theta_3) \end{aligned} \tag{18}$$
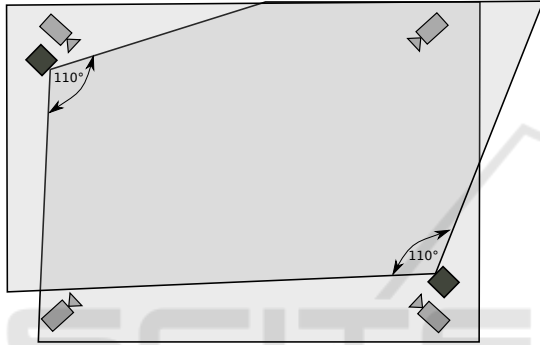
$$\begin{aligned} cos(\alpha_{AC}) = {} & sin(\theta_1) \cdot cos(\varphi_1) \cdot sin(\theta_3) \cdot cos(\varphi_3) \\ & + sin(\theta_1) \cdot sin(\varphi_1) \cdot sin(\theta_3) \cdot sin(\varphi_3) \\ & + cos(\theta_1) \cdot cos(\theta_3). \end{aligned} \tag{19}$$

Finally, Equations 10 to 12 can be solved using Newton's root finding method as presented in detail in (Islam et al., 2016). In the following section, the HTC

(a) Resulting tracking area of the Optitrack Prime 13 setup.

(b) Resulting tracking area of the HTC Lighthouse emitter.

Figure 7: Camera setup for the multi-view and the dual-axis rotating laser sweeps system.

Lighthouse system will be evaluated regarding tracking volume, accuracy, and applicability for mobile robots.

7.2 Experimental Setup

To evaluate the possible accuracy of the HTC Lighthouse system, an HTC Vive controller is equipped with an optically trackable rigid body. The rigid body is tracked by four Optitrack Prime 13 cameras. The cameras have a horizontal fov of $56°$ and a vertical fov of $46°$. The laser planes of the HTC Vive lighthouse emitter have a vertical and horizontal fov of 110 degrees. Figure 7 illustrates the camera placing including the opening angle of the different tracking solutions in a top-down view.

The setup for tracking the HTC Vive controller is presented in Figure 8. A rigid body consisting of six infrared marker is attached to the HTC Vive controller to validate the tracked trajectory's accuracy. In a second experiment, the controller is fixed on the Pioneer 2 robot to measure the robot's movement.
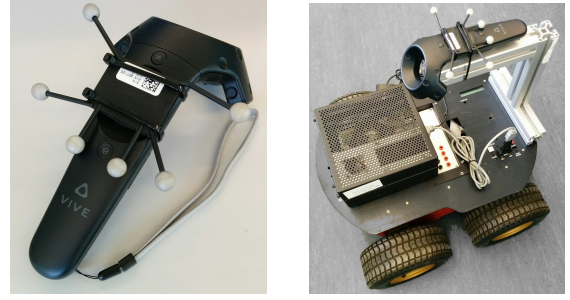
(a) Rigid setup of an HTC Vive controller and an optically trackable rigid body.

(b) Pioneer 2 Robot with attached trackable device accroding to Figure 8(a).

Figure 8: Tracked controller device and robot platform as used for evaluation.

7.3 Calibration

The tracking information of the HTC Vive is extracted using the Valve OpenVR library which merges the pose estimation based on the rotating laser sweeps with additional measurements of an inertial measurement unit.

The homogenous transformations $\mathbf{X}$ between the rigid body and the controller and $\mathbf{Z}$ between the infrared marker coordinate system and the dual-axis laser sweep coordinate system (see Figure 9) can be computed by solving the following equation:

$$\mathbf{A}_i\mathbf{X} = \mathbf{Z}\mathbf{B}_i$$
$$\begin{pmatrix}\mathbf{R}_{ai} & \mathbf{t}_{ai} \\ \mathbf{0} & 1\end{pmatrix}\begin{pmatrix}\mathbf{R}_x & \mathbf{t}_x \\ \mathbf{0} & 1\end{pmatrix} = \begin{pmatrix}\mathbf{R}_z & \mathbf{t}_z \\ \mathbf{0} & 1\end{pmatrix}\begin{pmatrix}\mathbf{R}_{bi} & \mathbf{t}_{bi} \\ \mathbf{0} & 1\end{pmatrix}. \quad (20)$$

The rotational and translational part in Equation 20 can be rearranged in the linear system:

$$\begin{pmatrix}\mathbf{R}_{ai}\otimes\mathbf{R}_{bi} & -\mathbf{I}_9 & \mathbf{0}_{9\times3} & \mathbf{0}_{9\times3} \\ \mathbf{0}_{3\times9} & \mathbf{I}_3\otimes\mathbf{t}_{bi}^T & -\mathbf{R}_{ai} & \mathbf{I}_3\end{pmatrix}\begin{pmatrix}vec(\mathbf{R}_x) \\ vec(\mathbf{R}_z) \\ \mathbf{t}_x \\ \mathbf{t}_z\end{pmatrix} \quad (21)$$
$$= \begin{pmatrix}\mathbf{0}_{9\times1} \\ \mathbf{t}_{ai}\end{pmatrix}.$$

Filling the position and orientation data from the measurement systems into $\mathbf{A}_i$ (HTC Vive Lighthouse) and $\mathbf{B}_i$ (Optitrack), Equation 21 can be solved in the least-square sense. Notice, that the controller has to undergo at least two independent general motions with nonparallel axes to retain a unique solution. Calibration was performed on 1000 measured poses within a sphere diameter of 70.46 mm. The overall mean pose error was 0.892 mm and 0.423°. With $\mathbf{X}$ and $\mathbf{Z}$ known, the following trajectories could be transformed into the same coordinate system and their position and rotation errors are calculated.
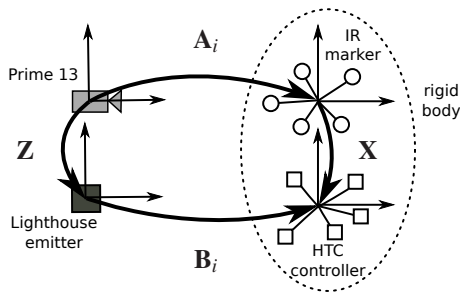
Figure 9: Geometric relation between the tracking **Z** and the rigid body **X** coordinate systems. $\mathbf{A}_i$,$\mathbf{B}_i$: Time varying measurement data.

7.4 Indoor and Outdoor Suitability

As an end consumer product for entertainment applications, the HTC Lighthouse is developed for indoor usage. Based on the expected interference due to direct sunlight, the photosensor signals will be strongly affected by noise. Additionally, a clear detection of the passing laser sweeps will probably not be possible in the presence of sunlight. Therefore, the system is not suited for outdoor applications.

7.5 Measurement Rate

The laser planes of the HTC Lighthouse rotate at 3600 *rpm*. Thus, a full rotation takes 16.66 *ms*. One laser sweep is completed in a half rotation and therefore takes 8.333 *ms*. The possible measurement rate for considering both sweeps of one emitter results in 60 *Hz*. Updating the pose every sweep, the update rate increases to 120 *Hz*. Because the sensor fusion algorithm implemented in the OpenVR library also uses an additional IMU for pose estimation, the resulting update rate is higher after sensor fusion.

7.6 Tracking Volumes

We determine the trackable volume by manually moving the tracked device within the measurement setups along the trajectory shown in Figure 10. The trajectory is grid-like to receive a good coverage of the volume. Since the illustration in Figure 10 only shows the received pose data from the measurement systems, gaps are indicating uncovered areas. As expected by the theoretical tracking area presented in Figure 7, the object could be tracked more robust and inside a larger volume using the HTC lighthouse system. Whereas the rigid body needs to be visible in at least two camera images to be tracked, the position of the controller can be computed only visible for one Lighthouse emitter. In contrast, the optical
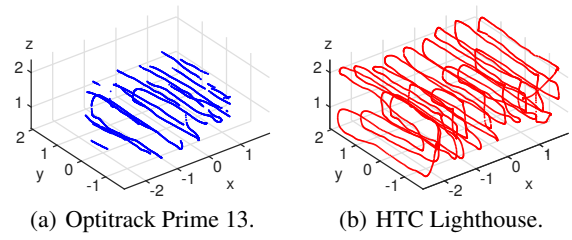

(a) Optitrack Prime 13.   (b) HTC Lighthouse.

Figure 10: Measured trajectories of the different setups.

(a) Optitrack Prime 13: $V_{ot} = 10.22\ m^3$.

(b) HTC Lighthouse: $V_{lh} = 27.02\ m^3$.
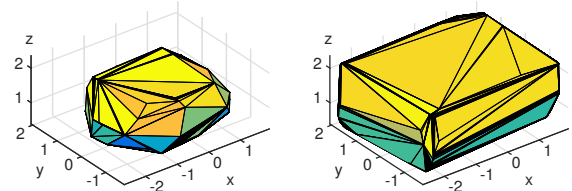
Figure 11: Convex tracking volume of the different setups.

system is more robust against occlusions supporting multiple points of view.

Figure 11 illustrates the tracking volume of the Optitrack Prime 13 cameras and the HTC Lighthouse systems. To get a measurable value to compare both systems, the convex volumes around the trajectories were calculated. Thereby we assume that the space within the trajectory-grid is measurable as well.

Comparing both volumes, we see that the HTC Lighthouse system is covering almost three times as much volume as the Optitrack system. That ratio is no constant value for all possible setups but underlines the effect for setups with limited space and cameras.

7.7 Accuracy

To determine the static and dynamic accuracy, the tracked device has been rigidly mounted on a Pioneer 2 robot. The resulting setup is shown in Figure 8. It must be taken into consideration that the quality of the calibration of Section 7.3 affects the dynamic and static trueness.

Static Accuracy: To determine the static accuracy, the robot has been placed statically on different positions inside the tracking volume near the center. The trueness and precision have then been computed, using the tracking information of the Optitrack Prime 13 setup as ground truth. The static accuracy is given in Table 1.

Dynamic Accuracy: The dynamic accuracy has been computed controlling the robot manually on the trajectories shown in Figure 12. As for the static accuracy, the Optitrack Prime 13 measurements are uses as ground truth.

Table 1 shows the precision and trueness of the

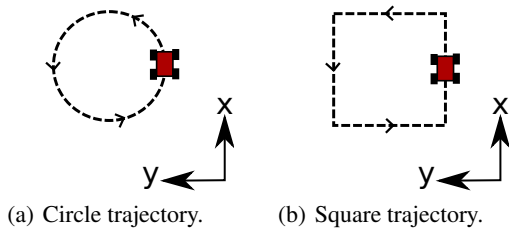(a) Circle trajectory.   (b) Square trajectory.

Figure 12: Experimental trajectories.

reconstructed trajectories tracked by the Optitrack Prime 13 setup and the HTC Lighthouse.

Table 1: Static and dynamic accuracy

	Position trueness [mm]	Position precision [mm]	Orientation trueness[°]	Orientation precision[°]
Static	1.699	0.361	0.353	0.008
Dynamic	1.615	0.433	0.291	0.046

Results: With a position trueness of 1.615 *mm* (static) and 1.699 *mm* (dynamic), the results are similar to the results given in (Burdea and Coiffet, 2003), which declare an RMS of 1.0 *mm* at a distance of 1.0 *m* for the similar Laserbild 2 system. Considering the larger average distance between the emitter and the tracking device in our setup, the measured accuracy also increases as expected. The dynamic and static position trueness are of a comparable magnitude. This can be reasoned by the relatively low speed of the robot compared to the measurement rate of the system.

8 CONCLUSION

In the first part of this paper, optical, acoustic, magnetic and inertial systems are compared regarding their principle of function. A summarizing comparison is given in Table 2.

The usage of the different tracking technologies strongly depends on the application which the system is needed for. Besides their line-of-sight limitation, optical tracking systems are proofed to be robust and to have a high accuracy. That is why stereo and multi-camera systems are typically used for commercial motion capture systems and are the standard in clinical applications (Birkfellner et al., 2008). Based on the widespread of mono cameras in handheld devices as smartphones, fiducial markers are currently state of the art for AR-applications. To improve the accuracy of these systems further, the results of fidu-

cial marker tracking are often combined using sensor fusion techniques with IMU data which are also state of the art in smartphone applications.

Magnetic tracking systems use AC or DC field coupling between source and sensor to determine the transformation between them. Therefore, no line-of-sight is required. As a restriction, magnetic systems are susceptible to conductive and ferromagnetic materials. The resulting magnetic field distortions worsen the trueness. A high resolution and precision can be obtained, but decreases rapidly with the distance.

Acoustic systems based on the duration of ultrasonic waves are too inaccurate to be used for accurate motion tracking. They are used in applications which do not require a high accuracy as in basic indoor navigation.

Inertial Systems are infrequently used as stand alone tracking solutions based on the occurring drift. Due to their low price microelectromechanical IMUs are often used as additional sensors.

Laser-based optical systems using rotating laser planes systems do have advantages, especially for virtual reality applications because of the high measurement rate and the low latency time (which is necessary to avoid motion sickness) and the possibility to realize position and orientation tracking on the same printed circuit board. Therefore, no additional time synchronization effort is necessary compared to combined devices for orientation and position tracking, such as external multi-view systems. In contrast to other optical systems, the usage of laser tracking based systems is less flexible, based on the higher marker complexity. Also, post processing is necessary to compute the position and the orientation based on the photodiode signals.

In the second part of this paper, it has been shown experimentally, that pose tracking using dual-axis rotating laser sweeps is a tracking solution which can cover a large tracking volume only using a small number of emitters. The experimentally evaluated static and dynamic accuracy is lower than the accuracy which can be achieved by commercial multi-camera setups. Nevertheless, the possible accuracy of the HTC Lighthouse system can be considered to be sufficient for many robotic applications.

REFERENCES

Abawi, D. F., Bienwald, J., and Dorner, R. (2004). Accuracy in optical tracking with fiducial markers: An accuracy function for artoolkit. In *Proceedings of the 3rd IEEE/ACM International Symposium on Mixed and Augmented Reality*, ISMAR '04, pages 260–261, Washington, DC, USA. IEEE Computer Society.

Table 2: Comparison of the presented methods.

Method	Typical Field of Application	Advantages	Disadvantages
Optical Single View	augmented reality applications	inexpensive, simple setup	line-of-sight necessary, small tracking volume
Optical Stereo View	instrument tracking in medical applications	high accuracy	line-of-sight necessary, small tracking volume
Optical Multi View	motion capturing systems, deformation analysis	high accuracy, less occlusions	line-of-sight necessary, expensive
Optical Laser	mobile robotics, head tracking, virtual reality applications	high accuracy	line-of-sight necessary, onboard processing required, tracked device needs additional electronics
Magnetic	body motion tracking, instrument tracking in medical applications	inexpensive, no line-of-sight necessary	affected by magnetic interference, tracked device needs additional electronics
Acoustic	rough localization using beacons, underwater localization	inexpensive	low accuracy, low measurement rate, affected by ultrasonic interference, tracked device needs additional electronics
Inertial	supplement to other applications applications using sensor fusion	tracking volume not limited, inexpensive, small, high measurement rate	position highly affected by drift, tracked device needs additional electronics

Andrew D. Wiles, D. G. T. and Frantz, D. D. (2004). Accuracy assessment and interpretation for optical tracking systems. In *In Medical Imaging 2004: Visualization, Image-Guided Procedures, and Display, Vol. 5367 pp. 421-432*.

Ascension Technology Corporation (2000). laserbird 2 - precision optical tracking. Internet.

Bergamasco, F., Albarelli, A., Rodol, E., and Torsello, A. (2011). Rune-tag: A high accuracy fiducial marker with strong occlusion resilience. In *CVPR*, pages 113–120. IEEE Computer Society.

Birkfellner, W., Hummel, J., Wilson, E., and Cleary, K. (2008). *Image-Guided Interventions*, chapter Tracking Devices, pages 23–44. Springer-Verlag.

Burdea, G. C. and Coiffet, P. (2003). *Virtual Reality Technology*. John Wiley and Sons. Inc.

Hightower, J. and Borriello, G. (2001). Location systems for ubiquitous computing. *Computer*, 34(8):57–66.

Hu, C., Meng, M.-H., and Mandal, M. (2007). A linear algorithm for tracing magnet position and orientation by using three-axis magnetic sensors. *IEEE Transactions on Magnetics*, 43(12):4096–4101.

Islam, S., Ionescu, B., Gadea, C., and Ionescu, D. (2016). Indoor positional tracking using dual-axis rotating laser sweeps. In *2016 IEEE International Instrumentation and Measurement Technology Conference Proceedings*, pages 1–6.

Mikko Kyt, Mikko Nuutinen, P. O. (2011). Method for measuring stereo camera depth accuracy based on stereoscopic vision. In *Three-Dimensional Imaging, Interaction, and Measurement, Conference Volume 7864*.

Noriega-Manez, R. J. (2007). Inertial navigation. Coursework for Physics 210, Stanford University, Autumn 2007.

NovAtel (2014). Imu errors and their effects. *APN-064*.

Paperno, E., Sasada, I., and Leonovich, E. (2001). A new method for magnetic position and orientation tracking. *IEEE Transactions on Magnetics*, 37(4 I):1938–1940.

Pentenrieder, K., Meier, P., Klinker, G., and Gmbh, M. (2006). Analysis of tracking accuracy for single-camera square-marker-based tracking. In *Proc. Dritter Workshop Virtuelle und Erweiterte Realität der GI-Fachgruppe VR/AR, Koblenz, Germany*.

Polhemus, I. (2017a). Fastrack - the fast and easy digital tracker. Internet. http://polhemus.com/_assets/img/FASTRAK_Brochure.pdf.

Polhemus, I. (2017b). Patriot wireless. Internet. http://polhemus.com/_assets/img/ PATRIOT_WIRELESS_brochure.pdf.

Priyantha, N. B., Chakraborty, A., and Balakrishnan, H. (2000). The cricket location-support system. In *Proceedings of the 6th Annual International Conference on Mobile Computing and Networking*, pages 32–43.

Raab, F., Blood, E., Steiner, T., and Jones, H. (1979). Magnetic position and orientation tracking system. In *IEEE Transactions on Aerospace and Electronic Systems*, volume 15.

Szeliski, R. (2010). *Computer Vision: Algorithms and Applications*. Springer-Verlag New York, Inc., New York, NY, USA, 1st edition.

Ward, A., Jones, A., and Hopper, A. (1997). A new location technique for the active office. *IEEE Personal Commun.*, 4(5):42–47.

Woodman, O. J. (2007). An introduction to inertial navigation. Technical Report UCAM-CL-TR-696, University of Cambridge, Computer Laboratory.